Air Force Institute of Technology
AFIT Scholar

Theses and Dissertations   Student Graduate Works

3-23-2018

Simulation and Modeling of High Energy Laser-Induced Droplet Shattering In Clouds

Andrew P. Lawrence

Follow this and additional works at: https://scholar.afit.edu/etd

Part of the Physical Sciences and Mathematics Commons

SIMULATION AND MODELING OF
HIGH ENERGY LASER-INDUCED
DROPLET SHATTERING IN CLOUDS

THESIS

Andrew P. Lawrence, 2d Lt, USAF

AFIT-ENC-MS-18-M-003

DEPARTMENT OF THE AIR FORCE
AIR UNIVERSITY

AIR FORCE INSTITUTE OF TECHNOLOGY

Wright-Patterson Air Force Base, Ohio

SIMULATION AND MODELING OF

HIGH ENERGY LASER-INDUCED

DROPLET SHATTERING IN CLOUDS

THESIS

Presented to the Faculty

Department of Applied Mathematics and Statistics

Graduate School of Engineering and Management

Air Force Institute of Technology

Air University

Air Education and Training Command

in Partial Fulfillment of the Requirements for the

Degree of Master of Science in Applied Mathematics

Andrew P. Lawrence, B.S.

2d Lt, USAF

February 28, 2018

AFIT-ENC-MS-18-M-003

SIMULATION AND MODELING OF

HIGH ENERGY LASER-INDUCED

DROPLET SHATTERING IN CLOUDS

THESIS

Andrew P. Lawrence, B.S.
2d Lt, USAF

Committee Membership:

Dr. Benjamin Akers, PhD
Chair

Dr. Steven Fiorino, PhD
Member

Maj Jonah Reeger, PhD
Member

AFIT-ENC-MS-18-M-003

Abstract

The process of a megawatt laser passing through a cloud is modeled. Specifically, the potential for droplet shattering is explored as a method for clearing a path through a cloud through which a second laser may be sent unobstructed. The paraxial approximation, an approximation to Maxwell's equations, is used to model the beam propagation. The simplified cloud model has assumed a distribution of pure, timescale restricted, droplets evenly distributed with uniform radius and initial temperature. All of the radiative heating is assumed to heat the droplet, neglecting radius change and vaporization based upon characteristic time scales. A 1+1 dimensional model is solved analytically over time and used to verify a numerical model which is then scaled up and applied to the 2+1-dimensional, radially symmetric case. The process is shown to create a cleared channel in a realistic amount of time given the constraining assumptions.

I would like to dedicate this work to my cohort in math through both my undergraduate and graduate degrees. His love for math has inspired me to work harder than I could have on my own. He has helped me through tough times and taught me how to be a bigger man. Quite literally.

Acknowledgements

I could not, in good conscience, complete this thesis without thanking my advisor, Dr. Ben Akers, for his guidance and instruction throughout the process of completing this thesis. He is a wealth of knowledge that helped me work through some of the toughest (and sometimes the simplest) concepts of this project. without his help, this document pale in comparison to what follows.

Andrew P. Lawrence

Table of Contents

SIMULATION AND MODELING OF

HIGH ENERGY LASER-INDUCED

DROPLET SHATTERING IN CLOUDS

I. Introduction

This document models the effect of self-induced atmospheric changes on the propagation of pulsed High Energy Lasers (HELs). Atmospheric laser propagation is an important aspect of many applications including targeting, wireless communication, energy transfer, remote sensing, the measurement of gravity waves, and many more [1, 2, 3, 4]. Specifically, the interactions between electromagnetic radiation and water droplets in the atmosphere are important to high-flux laser cloud-clearing. The use of HEL to clear clouds has been discussed by a number of authors over the past several years [5, 6, 7, 8, 9]. Experimental tests have measured the instability of droplets at high irradiances, demonstrated the clearing of ice crystal clouds, and achieved the clearing of stratus-like clouds [10, 11, 12, 13, 14]. There has also been theoretical research investigating how a prescribed beam affects cloud dynamics [15, 16, 17, 18] and how a prescribed cloud affects a dynamic beam [19, 20, 21]. Research has been done on coupling the beam dynamics with those of the cloud [22, 23, 24]. The model presented here will also couple the cloud and beam, but will use a 2+1 dimensional, radially symmetric model at high laser irradiances where evaporation is negligible.

In this work, a model to numerically simulate the propagation of pulsed wave HEL is developed in order to study the interplay between laser-induced droplet shattering and medium-based refractive index changes. This process can be visualized in Figure 1. The scale of laser wavelengths and beam propagation distance typically

differ by many orders of magnitude making direct simulations of the dynamics of the atmosphere unreasonable. The conventional approach is to use an envelope equation for the beam propagation such as the paraxial equation [25, 26, 27]. An envelope equation will be used as the basis for the laser model, but will also include refractive index terms which depend on the presence of water droplets or lack thereof. This coupling allows the beam to respond to the surrounding droplet medium and change accordingly.

The droplet dynamics depend on the deposition of energy by the incident laser. The droplets respond to the energy changes through a number of thermodynamic, and hydrodynamic processes, including vaporization, convection, conduction, and radiative heating. Stimulated Raman scattering and other nonlinear optical effects important in transparent droplets are negligible [28, 29, 18]. For high irradiances, the effects of conduction and convection are of negligible size, and the effects of vaporization increase but operate on a relatively slow characteristic time scale when compared to that of radiative heating and can be neglected as well [18, 30]. Thus, the time evolution of the droplet distribution depends only on temperature fluctuations within each droplet resulting from the radiative heat transfer from the laser. As the beam heats the droplets, hot spots are created due to nonuniform heating. This
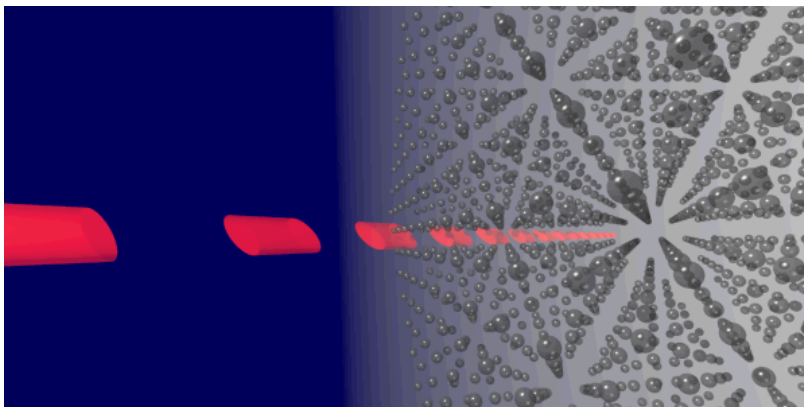

Figure 1. Visual model of a pulsed laser incident upon a distribution of droplets. Not to scale. (Courtesy of Dr. Ben Akers)

2

process is present in all laser radiative droplet heating, but is more pronounced at higher intensities [18, 31, 32]. Unlike liquid water at atmospheric pressures, the phase transition from liquid to vapor for suspended, pure, atmospheric droplets does not occur at 100°C [18, 33, 34]. Instead, the maximum temperature of the liquid phase is the critical temperature, $T_{crit} \approx 305°C$ [35], at which a sudden spontaneous nucleation of the vapor phase occurs. When hot spots cause the interior of the droplet to reach this critical temperature, the sudden vaporization causes the droplet to explode [28, 18, 36, 37].

For this analysis we consider a regime in which the incident laser flux is large enough to cause shattering ($>10^4$ W/cm^2), but not so large as to create plasma ($<10^8$ W/cm^2), given a laser wavelength of 10.6 μm [18, 38, 39, 40, 41]. Such a regime corresponds to rather high irradiances when considered in atmospheric propagation scenarios, but relatively small irradiances compared to the lasers often used in laboratory or industrial settings [42, 43, 44]. The U.S. Air Force operated Airborne Laser (ABL) was able to maintain a 10^6 W/cm^2 continuous-wave laser for seconds at a time [45]. An artificially induced pulse could be applied to this laser to achieve the desired pulse length. Other lasers exist that can achieve 10 megawatt peak irradiance over microsecond pulses with a rate of 200 pulses per second and are CO_2 based, which is necessary for producing the desired 10.6 μm wavelength [46]. Therefore, practical means are available which meet and exceed the desired specifications to induce droplet shattering.

When the irradiated droplets shatter, this analysis assumes that they leave behind a cleared zone within the larger spatial distribution of droplets that does not contain drops. Consequentially, the refractive index in this cleared domain will be different from the area containing droplets. This is assumed to be the only change to the refractive index; there is assumed to be no change based upon the temperature fluc-

3

tuation of the droplets or the surrounding vapor [18, 22, 47]. This piecewise change in the refractive index of the propagation medium feeds back upon the beam allowing it to penetrate further, heat up more drops, shatter them, and repeat.

The remainder of the paper is organized as follows. In section 2, we present the models used for simulation of the coupled beam and atmospheric dynamics. In section 3, we present the numerical methods and simulation results, including both spatial and temporal convergence studies. In section 4, we conclude and present future research areas.

II. Background

We will derive our model equations from first principles and describe the ansatz used to arrive at a closed form solution. But first, we will discuss the assumptions in our model.

First, let us review the assumptions concerning our cloud medium. A simple cloud consisting of a uniform distribution of droplets with constant initial radius, D_0, and temperature, T_0, will be assumed. The inclusion of nonuniform droplet radii would require absorption coefficients as a function of the laser wavelength to droplet size ratio and could be included in future research. A nonuniform initial temperature distribution would result in multiple droplet shattering fronts occurring within the cloud. The numerical scheme presented below could accommodate the more complicated initial condition, but a uniform initial temperature distribution is assumed for a simple, initial approach.

The droplets themselves are assumed to be perfect spheres which do not rotate or move; the time scale on which our laser is operating is significantly shorter than that of any potential velocity fields. The cloud is also assumed to consist only of gas and droplets. The droplets are assumed to be pure H_2O and contain no impurities. The droplets shatter instantaneously once any internal point reaches the critical temperature. The maximum temperature of each drop at a given location and time, $T_{max}(r, z, t)$, is sufficient to track when shattering will occur. The droplets do not to change radius on the time-scale of the droplet shattering. When a droplet is shattered it is assumed to be immediately replaced by vapor. The droplet radius distribution for all space and time can be represented by

$$D(r, z, t) = \begin{cases} D_0 & T_{max}(r, z, t) < T_{crit} \\ 0 & T_{max}(r, z, t) \geq T_{crit} \end{cases}$$

5

Next, we will outline the assumptions governing our laser. Our model will ignore any propagation in the backwards direction. We will assume that the propagation distance of our laser is large with respect to the beam width, an approximation which allows one to derive the paraxial approximation. Finally, the laser will be assumed collimated.

2.1 Paraxial Wave Equation

As we are modeling the propagation of a laser, we will begin our derivation of the laser equation with Maxwell's equations in a generic medium free of charge and current:

$$\nabla \cdot \mathbf{E} = 0 \tag{1a}$$

$$\nabla \cdot \mathbf{B} = 0 \tag{1b}$$

$$\nabla \times \mathbf{E} = -\frac{\partial \mathbf{B}}{\partial t} \tag{1c}$$

$$\nabla \times \mathbf{B} = \mu\epsilon\frac{\partial \mathbf{E}}{\partial t} \tag{1d}$$

In (**??**) ϵ and μ are the permitivity and permeability, respectively, of the propagation medium (in our case, a cloud).

We will now take the curl of Faraday's Law, equation (1c), to get

$$\nabla \times (\nabla \times \mathbf{E}) = \nabla \times (-\frac{\partial \mathbf{B}}{\partial t}) \tag{2}$$

Using the vector identity

$$\nabla \times (\nabla \times \mathbf{A}) = \nabla(\nabla \cdot \mathbf{A}) - \nabla^2\mathbf{A}$$

we can simplify the left hand side of equation (2) and, assuming that continuous

second partial derivatives of $\mathbf{E}$ and $\mathbf{B}$ exist, we can simplify the right hand side, leaving

$$\nabla(\nabla \cdot \mathbf{E}) - \nabla^2 \mathbf{E} = -\frac{\partial}{\partial t}(\nabla \times \mathbf{B}) \tag{3}$$

Substituting in equation (1a), simplifying the left hand side of equation (3), and using the equation (1d) gives

$$\nabla^2 \mathbf{E} = \frac{1}{v^2}\frac{\partial^2 \mathbf{E}}{\partial t^2} \tag{4}$$

where $v = \frac{1}{\sqrt{\mu_j \epsilon_j}}$ such that μ_j and ϵ_j depend on the medium.

Assuming a solution to equation (4) of the form

$$\mathbf{E} = E(r,z)e^{-i\omega t}\hat{e}_1$$

where ω is the frequency of our laser and $\hat{e}_1$ is the unit vector along z, we see that the time dependence falls out:

$$\nabla^2 \mathrm{E} = -\frac{1}{v^2}\omega^2 \mathrm{E}.$$

We can take advantage of the relevant governing physics to express the constant v, the speed of light in the propagation medium, in terms of the speed of light, c, and the medium index of refraction, n,

$$\nabla^2 \mathrm{E} = -\frac{n^2\omega^2}{c^2}\mathrm{E}.$$

Making use of the spatial frequency, $k = \frac{\omega}{c}$, we now have the wave equation in our given medium

$$\nabla^2 \mathrm{E} + k^2 n^2 \mathrm{E} = 0 \tag{5}$$

to which we propose a solution of the form

$$\mathrm{E} = A(r, z)e^{ikn_0 z}$$

where $e^{ikn_0 z}$ is the plane wave with amplitude A, $r = \varepsilon R$, and $z = \varepsilon^2 Z$. The plane wave is slowly varying as evidenced by the incorporation of ε into the spatial dependence. This is known as the paraxial approximation. The ε coefficients also represent the approximation that the laser varies less in the direction of propagation, z, than it does in the radial transverse direction, r. The solution is assumed to be radially symmetric. We define the index of refraction as

$$\begin{aligned}
n(r, z, t) &= n_0(r, z, t) + \varepsilon^2 n_1(r, z, t) \\
&= \eta_0(r, z, t) + i\beta_0(r, z, t) + \varepsilon^2(\eta_1(r, z, t) + i\beta_1(r, z, t)) \quad (6)
\end{aligned}$$

with the initial refractive index expressed through η_0 and changes in the refractive index due to the laser beams interaction with the medium represented by η_1. Similarly the initial absorptivity is represented by β_0 and variations thereupon are represented by β_1.

Plugging our solution into the wave equation, (5), assuming our laser is radially symmetric, only decays in the propagation direction, z, and radial transverse direction, r, and simplifying gives

$$\varepsilon^2 \left(\frac{1}{r}A_r + A_{rr} \right) e^{ikn_0 z} + \varepsilon^2 2ikn_0 A_z e^{ikn_0 z} - k^2 n_0^2 A e^{ikn_0 z} + \varepsilon^4 A_{zz} e^{ikn_0 z}$$

$$+ k^2 n_0^2 A e^{ikn_0 z} + \varepsilon^2 2k^2 n_0 n_1 A e^{ikn_0 z} + \varepsilon^4 k^2 n_1^2 A e^{ikn_0 z} = 0.$$

Let us now group terms on the same order of ε and drop the common exponential term. As expected, the $O(1)$ terms satisfy equation (5) on their own,

$$-k^2 n_0^2 A + k^2 n_0^2 A = 0.$$

Next, the $O(\varepsilon^2)$ terms give

$$\frac{1}{r} A_r + A_{rr} + 2k^2 n_0 n_1 A + 2ikn_0 A_z = 0.$$

Assuming the $O(\varepsilon^4)$ terms are negligible, this is the Schrödinger equation which is known in this context as the paraxial wave equation.

$$A_z = \left(\frac{i}{2kn_0} \left(\frac{\partial^2}{\partial r^2} + \frac{1}{r} \frac{\partial}{\partial r} \right) + ikn_1 \right) A$$

or

$$A_z = \left(\frac{i\eta_0 + \beta_0}{2k(\eta_0^2 + \beta_0^2)} \left(\frac{\partial^2}{\partial r^2} + \frac{1}{r} \frac{\partial}{\partial r} \right) + ik\eta_1 - k\beta_1 \right) A.$$

2.2   Index of Refraction

As in (6) we have separated the real and imaginary parts of the index of refraction. In order to appropriately model the physics of our system, the values of the index of refraction and absorption (and their first order corrections) must reflect a proportionality between the water in the droplets and the surrounding vapor, reflected here as a volume ratio. The effective ratio of water to vapor, then, is

$$P(r, z, t) = \frac{V_{drops}}{V} \frac{D(r, z, t)}{D_0} = 10^{-6} \frac{D(r, z, t)}{D_0}$$

from *Cloud Physics* [48]. Using the rule of mixtures [49], the coupled values then

take the form

$$\eta_0(r, z, t) = P(r, z, t)\eta_{0,H_2O} + (1 - P(r, z, t))\eta_{0,v}$$

$$\eta_1(r, z, t) = P(r, z, t)\eta_{1,H_2O} + (1 - P(r, z, t))\eta_{1,v}$$

$$\beta_0(r, z, t) = P(r, z, t)\beta_{0,H_2O} + (1 - P(r, z, t))\beta_{0,v}$$

$$\beta_1(r, z, t) = P(r, z, t)\beta_{1,H_2O} + (1 - P(r, z, t))\beta_{1,v}$$

where we have incorporated our cloud composition assumption stated previously.

2.3 Heat Equation

Over time, the droplets will undergo periods of heating, due to the laser, and cooling, due to thermal conduction. Given the assumption of spherical symmetry, the heating inside the droplet is approximated by

$$c\rho T_t = \nabla \cdot (K\nabla T) + f(\xi)|A| \tag{7}$$

$$f(\xi) = \frac{4\pi}{\lambda_0} S(\xi) Re(n) Im(n) \tag{8}$$

$$S(\xi) = \sqrt{\frac{3}{2\pi}} e^{\frac{-9}{2}(\xi - 0.9)^2} + 0.8 \tag{9}$$

where c is the specific heat of water, ρ is the density of water, K is the thermal conductivity, f defines the heat production distribution, and S is a normalized source function representing how much a 5 μm droplet is heated due to radiation as a function of one, normalized, internal space dimension, ξ, visually approximated from Armstrong [18] and seen in Figure 2.

In equation (7) above, the first term on the right side of the equation accounts for thermal diffusion, while the second term represents heat effects due to radiation. Following Armstrong, for intense radiation, the heating term will dominate the thermal
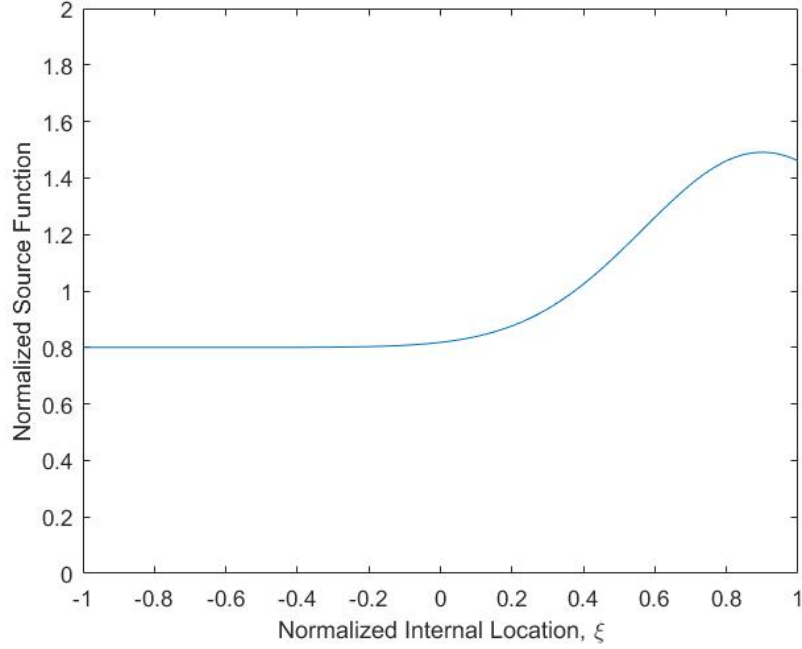
Figure 2. Normalized source function for $\lambda_0 = 10.6\ \mu$m and $D_0 = 5\ \mu$m along the droplet diameter parallel to the laser propagation direction of the incident laser beam (from left to right) sourced from Armstrong [18].

diffusion, a ratio of the two terms, set equal to one, and solved for a critical irradiance gives

$$|A|_{crit} = \frac{K\Delta T\lambda_0}{4\pi S(\xi)(\Delta D)^2 Re(n)Im(n)}.$$

Given a droplet radius of $D_0 = 5\ \mu$m and a laser wavelengths of $\lambda_0 = 10.6\ \mu$m, the critical irradiance is on the order of $10^4\frac{\text{W}}{\text{cm}^2}$. In order for the heating term to dominate and neglect diffusion, we consider a laser irradiance of at least $|A(0,0,t)| = 10^6\frac{\text{W}}{\text{cm}^2} = 1\frac{\text{MW}}{\text{cm}^2}$.

With a pulse laser of megawatt irradiance, the temperature equation becomes piecewise, the heating term dominating when the pulse is on, and being nonexistent

when the pulse is off, leaving the temperature to decay governed by the heat equation

$$c\rho T_t = \begin{cases} |A(r,z,t)|f(\xi) & \text{Pulse on} \\ KT_{\xi\xi} & \text{Pulse off} \end{cases}.$$

2.4 Heat equation boundary conditions

The heat equation in the cooling period can be solved numerically, once the boundary conditions have been determined. When evaluating the evolution of temperature between pulses, we no longer have a forcing function to dominate the heat dissipation and we are left with a simple heat equation

$$T_t = \frac{K}{c\rho}T_{\xi\xi}. \tag{10}$$

The boundary conditions for equation (10) prove more complex and take the following form [18]

$$-K\left.\frac{\partial T}{\partial \xi}\right|_{\xi=\Xi^-} = -K'\left.\frac{\partial T}{\partial \xi}\right|_{\xi=\Xi^+} + mL + mc(T-T_0) + \frac{m^3}{2\rho'^2}.$$

The term on the left-hand side of the equation is heat flux from inside the drop. On the right-hand side of the equation, the first term is the heat flux from the ambient water vapor outside of the drop, the second term is the energy used in vaporization on the surface, the third term is the energy loss due to droplet shrinking, and the last term is the convection term which represents the kinetic energy exchange [18].

As discussed earlier, the droplet shrinkage and convection are of negligible size, roughly one and two orders of magnitude smaller than the vaporization term, respectively. The vaporization term itself is negligible on the short time scale (μs) that droplet shattering takes place [18, 30]; in Armstrong, the vaporization term is shown

to cool droplets at a rate of $\approx 1\frac{\text{°C}}{\mu s}$ [18]. Assuming a constant heating at 50% efficiency over the period of a μs pulse, the rate of cooling at the beginning of the pulse off period will be $O(10^4)$, making the vaporization term negligible. The only term left is that of heat transfer leaving through the surface of the drop. Thus we approximate the boundary conditions as

$$\frac{\partial T}{\partial \xi}(-1,t) = \frac{\partial T}{\partial \xi}(1,t) = 0$$

which imply no heat loss on the surface of the droplet until the droplet shatters.

2.5   Model

Below is a collective list of the relevant governing equations.

$$A_z = \left(\frac{i\eta_0 + \beta_0}{2k(\eta_0^2 + \beta_0^2)} \left(\frac{\partial^2}{\partial r^2} + \frac{1}{r}\frac{\partial}{\partial r} \right) + ik\eta_1 - k\beta_1 \right) A$$

which is coupled with

$$\eta_0(r,z,t) = P(r,z,t)\eta_{0,H_2O} + (1 - P(r,z,t))\eta_{0,v}$$

$$\eta_1(r,z,t) = P(r,z,t)\eta_{1,H_2O} + (1 - P(r,z,t))\eta_{1,v}$$

$$\beta_0(r,z,t) = P(r,z,t)\beta_{0,H_2O} + (1 - P(r,z,t))\beta_{0,v}$$

$$\beta_1(r,z,t) = P(r,z,t)\beta_{1,H_2O} + (1 - P(r,z,t))\beta_{1,v}$$

given that

$$P(r,z,t) = 10^{-6} \frac{D(r,z,t)}{D_0}$$

when D is defined by

$$
D(r, z, t) = \begin{cases} D_0 & T_{max}(r, z, t) < T_{crit} \\ 0 & T_{max}(r, z, t) \geq T_{crit} \end{cases}
$$

and the droplet heating is defined by

$$
c\rho T_t = \begin{cases} |A(r, z, t)| f(u) & \text{Pulse on} \\ K T_{\xi\xi} & \text{Pulse off} \end{cases}
$$

where the heat distribution and source function are defined as

$$
f(\xi) = \frac{4\pi}{\lambda_0} S(\xi) Re(n) Im(n)
$$

and

$$
S(\xi) = \sqrt{\frac{3}{2\pi}} e^{\frac{-9}{2}(u-0.9)^2} + 0.8.
$$

A collection of parameter values can be found in the Appendix.

2.6 1+1 Dimensional Laser Equation

At this point we will explore the simplified case in which the transverse directions, here r, are ignored. The simplified laser equation only considering the propagation direction, z, becomes a linear, (piecewise) constant coefficient ODE of the form

$$
A_z = i(\alpha(z, t) + i\beta(z, t))A \tag{11}
$$

where $\alpha(z, t) = k\eta_1(z, t)$ and $\beta(z, t) = k\beta_1(z, t)$ are piecewise constant in z. As we proceed to find the solution to equation (11), the solution will be valid on the same piecewise support as $\alpha(z, t)$ and $\beta(z, t)$.

14

To find the general form of the solution to our 1+1 dimensional laser equation at a given time, t, we begin with the conjugate of equation (11)

$$\overline{A}_z = -i(\alpha - i\beta)\overline{A}. \tag{12}$$

Multiplying equation (11) by $\overline{A}$ and its conjugate, (12), by A gives

$$\overline{A}A_z = i(\alpha + i\beta)A\overline{A}$$

and

$$A\overline{A}_z = -i(\alpha - i\beta)A\overline{A}.$$

Adding those last two equations, (2.6) and (2.6), together and recognizing the product rule returns

$$|A|^2 = |A|^2(z=0)e^{-2\beta z}$$

or

$$|A| = |A|(z=0)e^{-\beta z}$$

which is our solution in space at a given time, t.

Now that we know the general form of our laser equation in 1+1 dimensions, we can specify what it looks like in the different regimes. Before time $t = t_{crit}(0)$ no drops have been shattered and the thus, β is only the absorptivity of the region containing droplets. After time $t = \tau$, we must consider the boundary of the cleared zone, $z_{crit}(t)$. For $z < z_{crit}(t)$ the laser travels through a cleared region and β is the absorptivity of vapor only. For $z > z_{crit}(t)$ the absorptivity is back to that of a droplet region, but we must account for the fact that the laser has already traveled a distance of $z_{crit}(t)$

in a cleared medium.

$$|A|(z) = \begin{cases} |A|(0)e^{-k\beta_{0,H_2O}z} & t < t_{crit}(0) \\ |A|(0)e^{-k\beta_{0,v}z} & z < z_{crit}(t) \\ |A|(0)e^{-k\beta_{0,v}z_{crit}(t)}e^{-k\beta_{0,H_2O}(z-z_{crit}(t))} & z > z_{crit}(t) \end{cases} \Bigg\} \quad t > t_{crit}(0)$$

We now consider the maximum temperature of the droplets at the interface, which is governed by the equation

$$T_t = C|A|(z,t) \tag{13}$$

where $C = \max_{\xi \in [-1,1]} f(\xi) = \frac{2\sqrt{2\pi}}{\lambda_0}\eta_{0,H_2O}\beta_{0,H_2O}$. Solving for temperature at the droplet interface,

$$T(z, t_{crit}(z)) = \int_0^{t_{crit}(z)} C|A|(z,t)dt \tag{14}$$

$$= t_{crit}(0)C|A|(0)e^{-k\beta_{0,H_2O}z} + e^{-k\beta_{0,H_2O}z}\int_{t_{crit}(0)}^{t_{crit}(z)} C|A|(0)e^{-k(\beta_{0,v}-\beta_{0,H_2O})z_{crit}(t)}dt.$$

It should be noted that the temperature along the droplet interface is $T(z, t_{crit}(z)) = T_{crit}$, by definition. Seeking to solve for t_{crit}, we differentiate equation (14) with respect to z yielding

$$\frac{dT}{dz} = 0 = - t_{crit}(0)k\beta_{0,H_2O}C|A|(0)e^{-k\beta_{0,H_2O}z} + C|A|(0)e^{-k(\beta_{0,v}-\beta_{0,H_2O})z_{crit}(t_{crit}(z))}e^{-k\beta_{0,H_2O}z}t'_{crit}(z)$$

$$- k\beta_{0,H_2O}e^{-k\beta_{0,H_2O}z}\int_{t_{crit}(0)}^{t_{crit}(z)} C|A|(0)e^{-k(\beta_{0,v}-\beta_{0,H_2O})z_{crit}(t)}dt. \tag{15}$$

Let $u = z_{crit}(t)$. Then $du = z'_{crit}(t)dt$. Since z_{crit} and t_{crit} are inverse functions of one another, $t_{crit}(u) = t_{crit}(z_{crit}(t)) = t$ making $u = z_{crit}(t_{crit}(u))$ and

16

$du = z'_{crit}(t_{crit}(u))dt$. Thus, equation (15) becomes

$$0 = -t_{crit}(0)k\beta_{0,H_2O} + e^{-k(\beta_{0,v} - \beta_{0,H_2O})z}t'_{crit}(z) - k\beta_{0,H_2O}\int_0^z e^{-k(\beta_{0,v} - \beta_{0,H_2O})u}\frac{du}{z'_{crit}(t_{crit}(u))}.$$

$$(16)$$

But since

$$u = z_{crit}(t_{crit}(u))$$
$$\frac{d}{du}u = \frac{d}{du}z_{crit}(t_{crit}(u))$$
$$1 = z'_{crit}(t_{crit}(u))t'_{crit}(u),$$

equation (16) simplifies to

$$0 = -t_{crit}(0)k\beta_{0,H_2O} + e^{-k(\beta_{0,v} - \beta_{0,H_2O})z}t'_{crit}(z) - k\beta_{0,H_2O}\int_0^z e^{-k(\beta_{0,v} - \beta_{0,H_2O})u}t'_{crit}(u)du.$$

$$(17)$$

Differentiating with respect to z

$$0 = -k(\beta_{0,v} - \beta_{0,H_2O})e^{-k(\beta_{0,v} - \beta_{0,H_2O})z}t'_{crit}(z) + e^{-k(\beta_{0,v} - \beta_{0,H_2O})z}t''_{crit}(z) - k\beta_{0,H_2O}e^{-k(\beta_{0,v} - \beta_{0,H_2O})z}t'_{crit}(z)$$

and simplifying leaves a linear, constant-coefficient differential equation

$$k\beta_{0,v}t'_{crit}(z) = t''_{crit}(z)$$

to which the solution is known to be exponentials

$$t'_{crit}(z) = t'_{crit}(0)e^{k\beta_{0,v}z}.$$

$$(18)$$

17

Integrating equation (18) to solve for $t_{crit}(z)$ gives

$$t_{crit}(z) = \frac{t'_{crit}(0)}{k\beta_{0,v}} e^{k\beta_{0,v}z} + H$$

where H is a constant of integration that, once solved for, leaves

$$t_{crit}(z) = \frac{t'_{crit}(0)}{k\beta_{0,v}} e^{k\beta_{0,v}z} + t_{crit}(0) - \frac{t'_{crit}(0)}{k\beta_{0,v}}.$$

Evaluating equation (17) at $z = 0$ returns $t'_{crit}(0)$ in terms of $t_{crit}(0)$ returns

$$t'_{crit}(0) = t_{crit}(0)k\beta_{0,H_2O}.$$

The closure for $t_{crit}(0)$ can be found from the heat equation by taking advantage of the fact that the laser is constant in time on the interval $0 \leq t \leq t_{crit}(0)$. Thus

$$t_{crit}(0) = \frac{T_{crit}}{|A(0,0)|\, C}.$$

Finally,

$$t_{crit}(z) = \frac{T_{crit}}{|A(0,0)|\, C} \left(\frac{\beta_{0,H_2O}}{\beta_{0,v}} \left(e^{k\beta_{0,v}z} - 1 \right) + 1 \right). \tag{19}$$

Equation (19) can be inverted to produce

$$z_{crit}(t) = \frac{1}{k\beta_{0,v}} \ln\left[\frac{\beta_{0,v}}{\beta_{0,H_2O}} \left(\frac{t|A(0,0)|\, C}{T_{crit}} - 1 \right) + 1 \right]. \tag{20}$$

The equations for z_{crit} and t_{crit} can be used to predict the required time to penetrate a cloud of some depth or the depth penetrated at a given time given the laser irradiance, heating profile and critical temperature of water. Figure 3 shows $t_{crit}(z)$ including labels denoting where droplets are and are not.
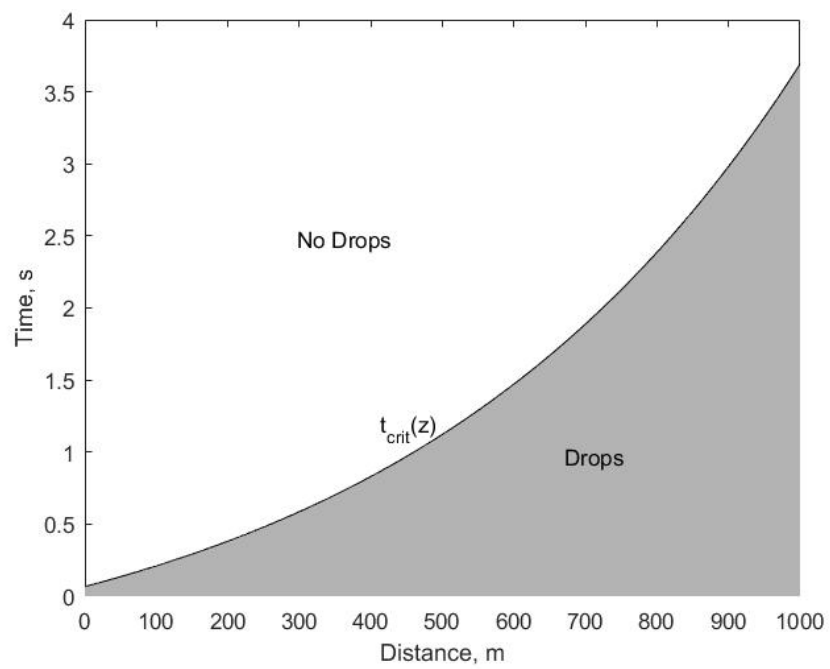
Figure 3. The time of the shattering droplet front as a function of distance through the cloud. The cleared area is labeled along with the remaining droplets.

III. Numerical Results

3.1 Numerical Method

For the 2+1-dimensional, radially symmetric case, the governing equations will be solved numerically. The laser equation in space will be solved first, for a fixed time, using the Crank-Nicholson scheme with zero boundary conditions [50]. Then the temperature equation will be solved with the laser irradiance just found using Euler's method. The droplet distribution is updated next, based on the temperature solution. The entire scheme is visualized in the flow chart in Figure 4 and repeated for the duration of a pulse. Between pulses, the built up heat in the droplets is the only dynamic variable in the system. Thus the heat equation governs that heat dissipation; it is modeled in one dimension and is solved using the Crank-Nicholson scheme. [50]

The scheme ends when the laser has penetrated the cloud. A channel is considered to be sufficiently cleared once all of the drops along the azimuthal axis, z, have been shattered. Additional clearing of droplets at the far side of the cloud, the maximum z distance, may occur due to the discretization in time. The last azimuthal drop can only be assessed to have been shattered at the end of a time step, allowing for the clearing of additional drops after the last azimuthal drop has shattered but before the time step is over. This effect can be seen in Figure 11 as the width of the cleared channel at the maximum z distance is wider than Δr, the transverse spatial resolution.

Parameters, such as pulse length and irradiance, are chosen to satisfy the underlying assumptions of our model. As discussed earlier, an irradiance between 10^4 W/cm^2 and 10^8 W/cm^2 is necessary to avoid plasma formation while allowing shattering to dominate droplet dynamics. Our model will use an irradiance of 10^6 W/cm^2. Given a wind speed of 30 mph and a cleared channel width of 1 m, the assumption of station-
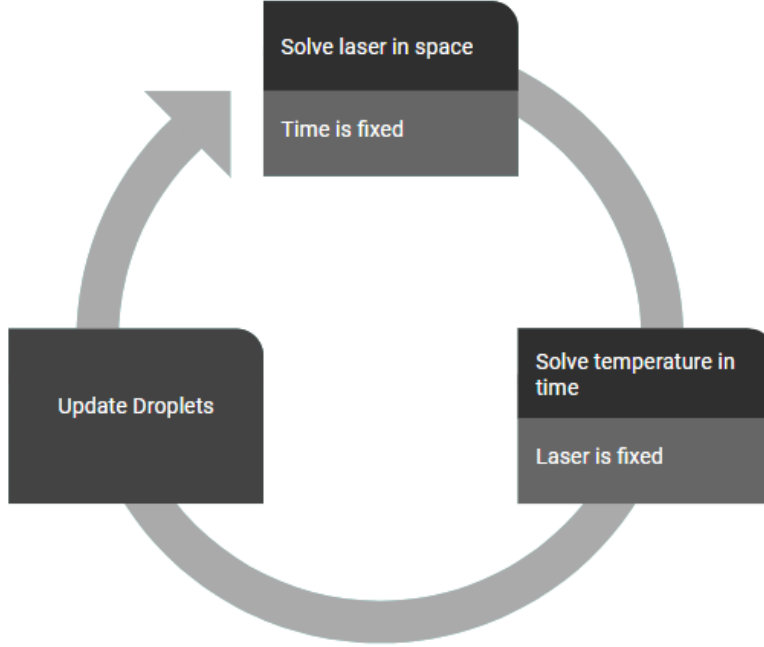
Figure 4. First the laser equation is solved in space. Then the temperature is solved for using the previously found laser irradiance. Then the droplet distribution is updated using the temperature. This process is repeated for the duration of a pulse.

ary droplets with respect to the laser effects only holds true if the laser can penetrate in less than 0.0357 seconds. That is the time it takes for a droplet to cross half the diameter of the cleared channel. Our model also maintains an implicit assumption that the laser acts on the entire cloud at once (the front of the laser entering the cloud is not tracked). Therefore, given a reasonable cloud depth of 100 m [48], the pulse must be no shorter than $3*10^{-7}$ s or 0.3 μs (and preferably an order of magnitude longer). Based on these restrictions and specifications of an existing laser system given in Gas Lasers [46], the laser model will operate with a pulse on time of $t_{on} = 4.185 \times 10^{-6}$ s, a pulse off time of $t_{off} = 8.069 \times 10^{-4}$ s, a 1.25 kHz rate, and MW/cm2 irradiance.

For numerical accuracy, the laser irradiance will be normalized, $\tilde{A} = \frac{A}{\|A\|_\infty}$. The laser equation will remain unchanged:

$$\tilde{A}_z = \left(\frac{i\eta_0 + \beta_0}{2k(\eta_0^2 + \beta_0^2)} \left(\frac{\partial^2}{\partial r^2} + \frac{1}{r} \frac{\partial}{\partial r} \right) + ik\eta_1 - k\beta_1 \right) \tilde{A}.$$

21

A time scale will be introduced in the temperature equation when the pulse is on to account for the normalization. Here we include c and ρ in the time scale while the pulse is on, $\tau_{on} = \frac{\|A\|}{c\rho} t_{on}$. A different time scale will be used when the pulse is off accounting just for K, c and ρ, $\tau_{off} = \frac{K}{c\rho} t_{off}$.

$$T_{\tau_{on}} = |\tilde{A}| f(u)$$

$$T_{\tau_{off}} = T_{\xi\xi}.$$

We will transform the results back to unscaled times after the simulation for reporting purposes.

3.2   Convergence Studies

As was discussed in Section 2.6, the 1+1 dimensional system has an explicit solution for all space and time. The exact solution can be used to verify the accuracy of the numerical scheme by implementing it in the 1+1 dimensional case and comparing the results. The numerical scheme is shown to solve the system and is visualized over all z and at discrete scaled times in Figure 5. Slices in time of the laser irradiance over space are shown for the duration of the laser. An initial high decay rate is seen as the laser is attenuated by the droplets, until the first drop shatters. From that time on, there is an initial low decay rate in the domain with only vapor, and then a change back to the droplet domain and a high decay rate.

By nature of the discretization of the domain onto a grid and the necessity of the scheme to round the location of the droplet front to either the left or the right of the interval in which the exact location exists, the scheme will introduce an error on the order of the spatial step size, $O(\Delta z)$. It is interesting to note in Figures 6 and 7 that the space and time interdependency of our model introduces an error on the order
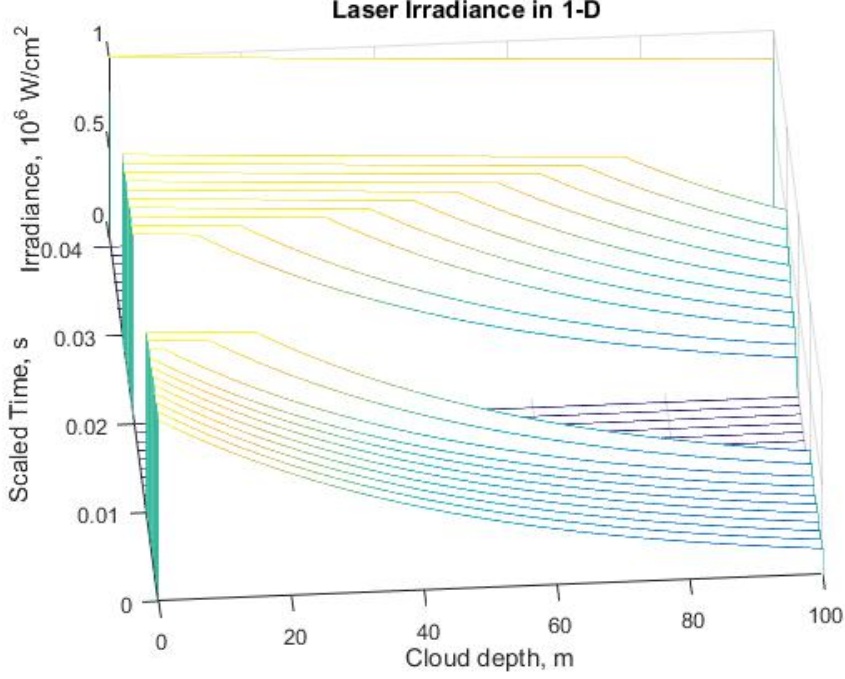
22

Figure 5. The irradiance of the laser for all z at discrete times in 1+1 dimensions. The pulse on length was $\tau_{on} = 4.185 \times 10^{-6}$ s, the pulse off time was $\tau_{off} = 8.069 \times 10^{-4}$ s, and the cloud depth used was 100 m.

of the time step size, $O(\Delta\tau)$, due to the $O(\Delta z)$ discussed above even when a second order, $O(\Delta\tau^2)$, integration scheme (Trapezoidal method) is used.

Following are convergence plots of the Cauchy error (Figures 6 and 8) and forward error (Figures 7 and 9) in both time (Figures 6 and 7) and space (Figures 8 and 9) demonstrating that the error is $O(\Delta\tau, \Delta z)$ as expected. In both space and time, the Cauchy error and forward error decay toward zero. Here, the Cauchy error is defined as

$$E_{C_j} = \left\| \left| A_{\Delta z_j}(z, \tau') \right| - \left| A_{\Delta z_{j-1}}(z, \tau') \right| \right\|_\infty$$

and the forward error is defined as

$$E_{F_j} = \left\| \left| A(z, \tau') \right| - \left| A_{\Delta z_j}(z, \tau') \right| \right\|_\infty$$

where $\left| A_{\Delta z_j}(z, t') \right|$ is the irradiance of the laser for all z and fixed time τ' found by

23

the numerical scheme using the jth step size. The laser equation was solved until time $\tau' = 0.01$ s with $\Delta z = 0.01$ m for the convergence study in time, and until $\tau' = 0.0100374$ s with $\Delta\tau = 10^{-7}$ s for the convergence study in space.
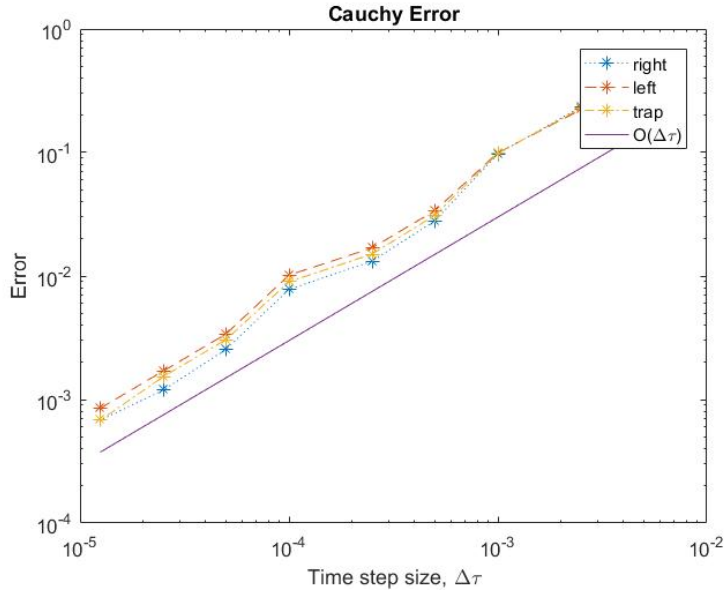
Figure 6. A convergence study in time of the Cauchy error of the numerical scheme in 1+1 dimensions for different integration schemes at time $\tau' = 0.01$ s. The Cauchy error is defined as $E_{C_j} = \left\|\left|A_{\Delta z_j}(z,\tau')\right| - \left|A_{\Delta z_{j-1}}(z,\tau')\right|\right\|_\infty$, represented by asterisks connected by dots for the right hand method, dashes for the left hand method, and dots and dashes for the trapezoidal method, and decays like $O(\Delta\tau)$.
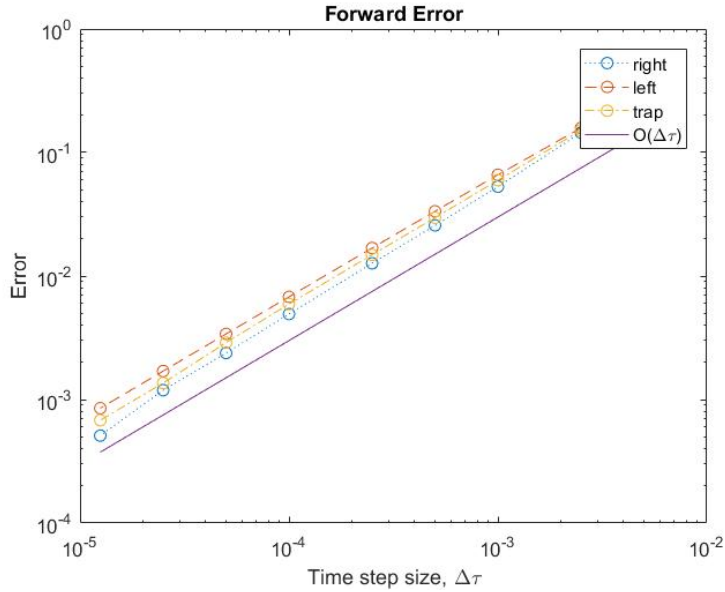

Figure 7. A convergence study in time of the forward error of the numerical scheme in 1+1 dimensions for different integration schemes at time $\tau' = 0.01$ s. The forward error is defined as $E_{F_j} = \left\|\left|A(z,\tau')\right| - \left|A_{\Delta z_j}(z,\tau')\right|\right\|_\infty$, represented by circles connected by dots for the right hand method, dashes for the left hand method, and dots and dashes for the trapezoidal method, and decays like $O(\Delta\tau)$.
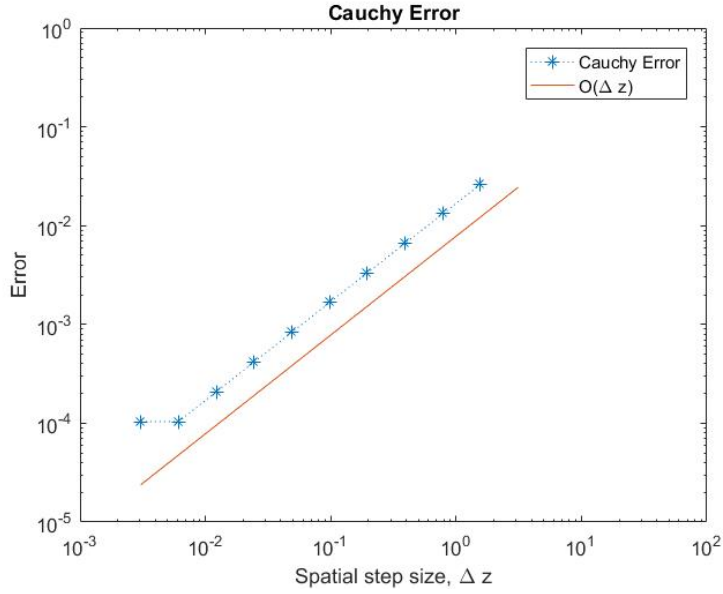
Figure 8. A convergence study in space of the Cauchy error of the numerical scheme in 1+1 dimensions at time $\tau' = 0.0100374$ s. The Cauchy error is defined as $E_{C_j} = \left\lVert \left\lvert A_{\Delta z_j}(z, \tau') \right\rvert - \left\lvert A_{\Delta z_{j-1}}(z, \tau') \right\rvert \right\rVert_\infty$. The error values are represented by asterisks and decay like $O(\Delta z)$.
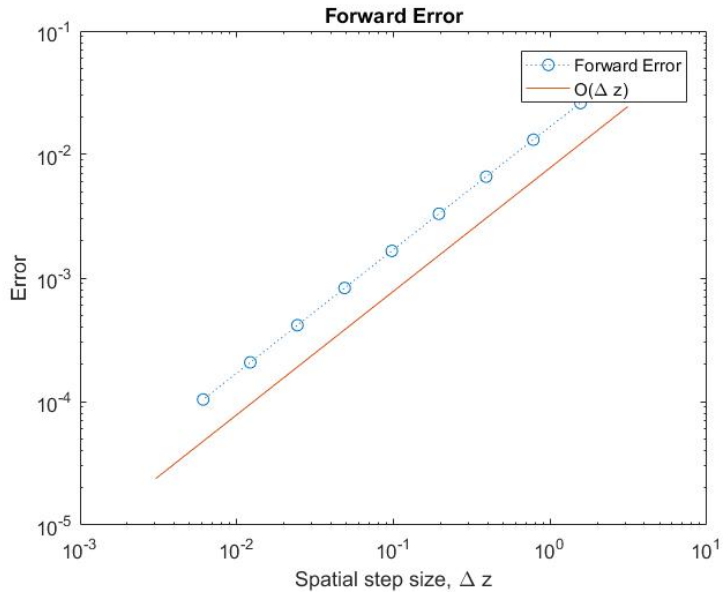

Figure 9. A convergence study in space of the forward error of the numerical scheme in 1+1 dimensions at time $\tau' = 0.0100374$ s. The Cauchy error is defined as $E_{F_j} = \left\lVert \left\lvert A(z, \tau') \right\rvert - \left\lvert A_{\Delta z_j}(z, \tau') \right\rvert \right\rVert_\infty$. The error values are represented by circles and decay like $O(\Delta z)$.

26

3.3 2+1 Dimensional, Radially Symmetric Laser Equation Simulation

We can finally solve the full governing system including the original 2+1-dimensional, radially symmetric PDE confident that our splitting scheme works. Figure 10 shows the laser irradiance over two-dimensional, radially symmetric space for times $t = 0.0008$ s (after the first pulse and cooling period) and $t = 0.0016$ s (the final time) and Figure 11 shows the maximum temperature within each drop over two-dimensional, radially symmetric space for the same times. The laser is found to have penetrated the cloud after 2 pulses and $t = 0.0016$ seconds which is an order of magnitude smaller than the 0.0357 seconds necessary to satisfy our assumptions.
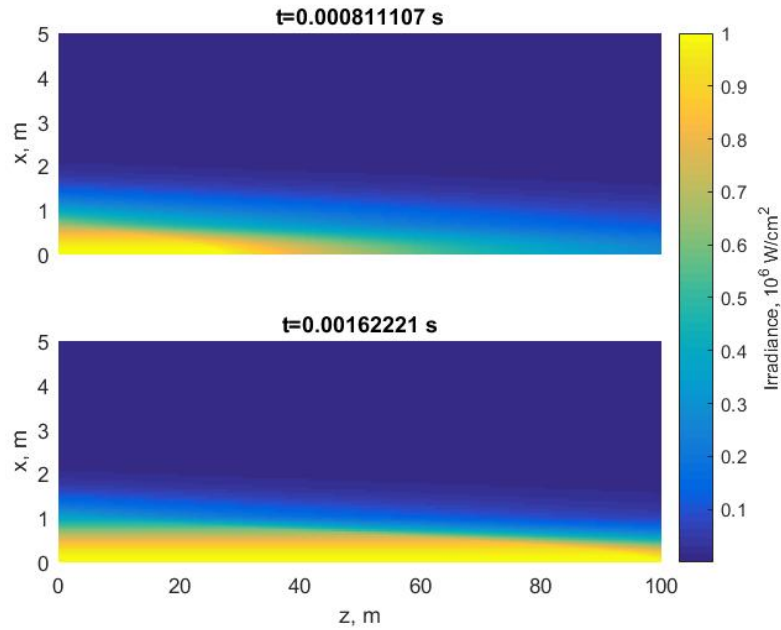
Figure 10. The irradiance of the laser over two-dimensional, radially symmetric space for times $t = 0.0008$ and 0.0016 s. The pulse on time was $t_{on} = 4.185 \times 10^{-6}$ s, the pulse off time was $t_{off} = 8.069 \times 10^{-4}$ s, and the cloud depth was 100 m.

Figure 11. The maximum temperature within each droplet over two-dimensional, radially symmetric space for times $t = 0.0008$ and 0.0016 s. The pulse on time was $t_{on} = 4.185 \times 10^{-6}$ s, the pulse off time was $t_{off} = 8.069 \times 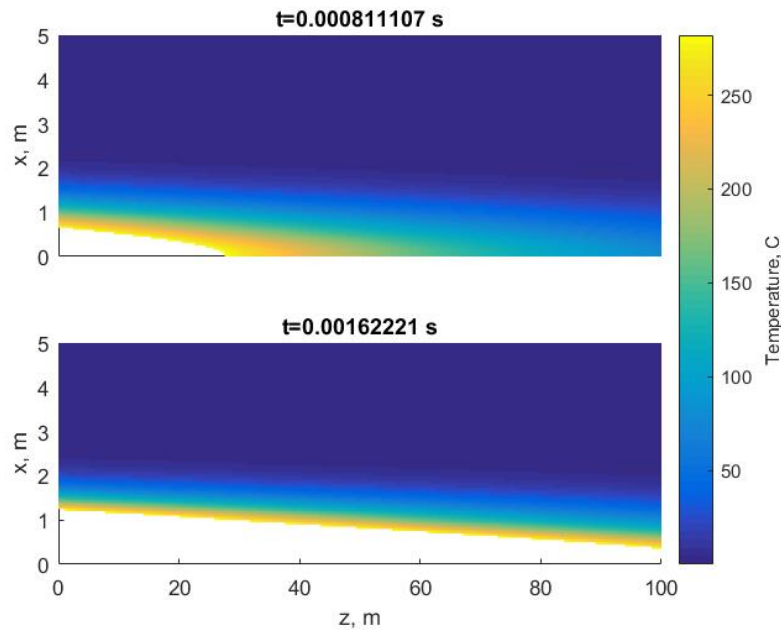10^{-4}$ s, and the cloud depth was 100 m. The white space is used to represent the cleared channel where the droplets have been shattered.

28

IV. Conclusions and Future Research

The model described above has simulated the process of a pulsed, high-energy laser directed toward a cloud. The constituent droplets are heated to a critical temperature at which they shatter, leaving a cleared space. Over time, this process creates a cleared channel in the cloud through which another laser can be sent unobstructed. The model used, however, was very simplified and intended, primarily as a proof of concept. The inclusion of water vapor dynamics would make the model more realistic, to include pluming and turbulence. Specifically, tracking the vapor temperature would be a natural and straightforward extension of this work.

The inclusion of nonuniform droplet radii and nonuniform initial temperature distribution are also opportunities for future research, as well as is a model for lower values of laser irradiance. While the high intensities necessary for this model are attainable, it is far more practical to use lower regime. Therefore, it would be interesting to develop a model for the lower irradiances in which effects such as evaporation, ablation and vaporization dominate droplet dynamics. Fluid effects within the droplets are likely to become more important in the lower regime levels.

While the model presented demonstrates that this effect is limited to small clouds (100 m), some military conclusions can still be drawn. Aircraft can use large clouds to hide behind without worry of adversary lasers reaching them. Conversely, an aircraft can hide visually behind a small cloud while still affecting what is on the other side.

In conclusion, this project proved, in concept, that the high energy, droplet shattering approach to laser induced cloud clearing is possible. A numerical simulation is provided, along with analytical equations for predicting the required time to penetrate a cloud of given depth.

Appendix

Parameter values

$$\lambda_0 = 10.6 \times 10^{-6} \quad \text{m}$$

$$k = \frac{2\pi}{\lambda_0} \quad \text{m}^{-1}$$

$$\rho = 10^3 \frac{\text{kg}}{\text{m}^3}$$

$$c = 4.1855 \times 10^3 \frac{\text{J}}{\text{kg} \cdot {}^\circ\text{C}}$$

$$K = 5.187 \times 10^{-2} \frac{\text{J}}{\text{s} \cdot \text{m} \cdot {}^\circ\text{C}}$$

$$\eta_{0,H_2O} = 1.179$$

$$\eta_{1,H_2O} = 0.776405$$

$$\eta_{0,v} = 1$$

$$\eta_{1,v} = 3.64807 * 10^{-6}$$

$$\beta_{0,H_2O} = 0.07558$$

$$\beta_{1,H_2O} = 0.03$$

$$\beta_{0,v} = 0.003 \times 10^{-3}$$

$$\beta_{1,v} = 0.003 \times 10^{-9}$$

Bibliography

1. L. C. Andrews and R. L. Phillips, *Laser beam propagation through random media*, vol. 1. SPIE press Bellingham, WA, 2005.

2. K. N. Liou, S.-C. Ou, Y. Takano, and J. Cetola, "Remote sensing of three-dimensional cirrus clouds from satellites: application to continuous-wave laser atmospheric transmission and backscattering," *Applied optics*, vol. 45, no. 26, pp. 6849–6859, 2006.

3. R. J. Bartell, G. P. Perram, S. T. Fiorino, S. N. Long, M. J. Houle, C. A. Rice, Z. P. Manning, D. W. Bunch, M. J. Krizo, and L. E. Gravley, "Methodology for comparing worldwide performance of diverse weight-constrained high energy laser systems," in *Proc. of SPIE Vol*, vol. 5792, p. 77, 2005.

4. B. P. Abbott, R. Abbott, R. Adhikari, P. Ajith, B. Allen, G. Allen, R. S. Amin, S. B. Anderson, W. G. Anderson, M. A. Arain, and others, "LIGO: the laser interferometer gravitational-wave observatory," *Reports on Progress in Physics*, vol. 72, no. 7, p. 76901, 2009.

5. R. L. Armstrong, S. A. W. Gerstl, and A. Zardecki, "Nonlinear pulse propagation in the presence of evaporating aerosols," *Journal of the Optical Society of America*, vol. 2, no. 10, pp. 1739–1746, 1985.

6. K. D. Egorov, V. P. Kandidov, and S. S. Chesnokov, "Numerical analysis of the propagation of high-intensity laser radiation in the atmosphere," *Soviet Physics Journal*, vol. 26, pp. 161–173, 2 1983.

7. A. V. Kuzikovski, L. K. Chistyakova, and V. I. Kokhanov, "Pulsed clearing of a synthetic aqueous aerosol by CO2 laser radiation," *Soviet Journal of Quantum Electronics*, vol. 11, no. 10, pp. 1277–1281, 1981.

8. V. E. Zuev and Y. D. Kopytin, "Nonlinear propagation of intense light in a gaseous medium with solid microfilling," *Soviet Physics Journal*, vol. 20, pp. 1458–1479, 11 1977.

9. R. J. Lipinski and R. F. Walter, "Hole-Boring through Clouds for Laser Power Beaming," in *SPIE 2376, Laser Power Beaming II*, vol. 2376, p. 9, SPIE Proceedings, 1995.

10. J. G. Xie, T. E. Ruekgauer, R. L. Armstrong, and R. G. Pinnick, "Evaporative instability in pulsed laser-heated droplets," *Physical Review Letters*, vol. 66, no. 23, pp. 2988–2991, 1991.

11. A. P. Waggoner, L. F. Radke, V. Buonadonna, and D. R. Dowling, "Cloud Clearing with a CO2-Laser in a Cirrus Cloud Simulation Facility," *Appl. Optics.*, vol. 31, no. 27, pp. 5871–5877, 1992.

12. G. P. Quigley, R. B. Webster, E. J. Caramana, R. L. Morse, and G. W. York, "Cloud hole boring with long pulse CO(2) lasers: theory and experiment.," *Applied optics*, vol. 30, no. 21, pp. 3041–6, 1991.

13. E. J. Caramana, J. L. Kindel, R. L. Morse, G. P. Quigley, R. B. Webster, and G. W. York, "Droplet Shattering, Vaporization and Recondensation in Cloud Clearing with Long Pulse Infrared Chemical Lasers," tech. rep., 1990.

14. M. Autric, P. Vigliano, D. Dufresne, J. P. Caressa, and P. Bournot, "Pulsed CO2 Laser-Induced Effects on Water Droplets," *AIAA Journal*, vol. 26, no. 1, pp. 65–71, 1988.

15. G. Caledonia and J. Teare, "Laser Beam-Hygroscopic Baam-Hygroscopic Aerosol Interactions," *Journal of Heat Transfer*, vol. 99, no. May 1977, pp. 281–286, 1977.

16. R. L. Armstrong, "Interactions of absorbing aerosols with intense light beams," *Journal of Applied Physics*, vol. 56, no. 7, pp. 2142–2153, 1984.

17. F. A. Williams, "On vaporization of mist by radiation," *International Journal of Heat and Mass Transfer*, vol. 8, no. 4, pp. 575–587, 1965.

18. B.-S. Park and R. L. Armstrong, "Laser droplet heating: fast and slow heating regimes.," *Applied Optics*, vol. 28, no. 17, pp. 3671–3680, 1989.

19. D. R. Johnston and D. E. Burch, "Attenuation by Artificial Fogs in the Visible , Near Infrared , and Far Infrared," vol. 6, no. 9, pp. 1497–1501, 1967.

20. M. M. Colavita, M. R. Swain, R. L. Akeson, C. D. Koresko, and R. J. Hill, "Effects of Atmospheric Water Vapor on Infrared Interferometry," *Publications of the Astronomical Society of the Pacific*, vol. 116, no. 823, pp. 876–885, 2004.

21. H. Matsumoto, "The refractivities of water vapour for CO2 laser lines," *Optics Communications*, vol. 50, pp. 356–358, 7 1984.

22. S. M. Chitanvis and S. A. W. Gerstl, "Aerosol clearing model for a high-energy laser beam propagating through vaporizing media," *Journal of Applied Physics*, vol. 62, no. 8, pp. 3091–3096, 1987.

23. C. T. Lee, T. G. Miller, and R. W. Jones, "Fog dispersal by CO 2 laser pulses: an exact solution including prevaporization heating," *Applied optics*, vol. 21, no. 3, pp. 428–432, 1982.

24. A. H. Aitken, J. N. Hayes, and P. B. Ulrich, "Propagation of High-Energy 10 . 6-Micron Laser Beams Through the Atmosphere," tech. rep., 1971.

25. M. J. Ablowitz, *Nonlinear Dispersive Waves: Asymptotic Analysis and Solitons*, vol. 47. Cambridge University Press, 2011.

26. C. Sulem and P.-L. Sulem, *The nonlinear Schrödinger equation: self-focusing and wave collapse*, vol. 139. Springer Science & Business Media, 2007.

27. D. G. Fouche, C. Higgs, and C. F. Pearson, "Scaled atmospheric blooming experiments (SABLE)," *The Lincoln Laboratory Journal*, vol. 5, no. 2, pp. 273–293, 1992.

28. R. G. Pinnick, A. Biswas, G. Fernández, P. Chlek, R. L. Armstrong, H. Latifi, E. Creegan, V. Srivastava, and M. Jarzembski, "Stimulated Raman scattering in micrometer-sized droplets:time-resolved measurements," *Optics Letters*, vol. 13, p. 494, 6 1988.

29. J.-Z. Zhang, D. H. Leach, and R. K. Chang, "Photon lifetime within a droplet: temporal determination of elastic and stimulated Raman scattering," *Optics Letters*, vol. 13, p. 270, 4 1988.

30. E. J. Caramana, R. B. Webster, G. P. Quigley, and R. L. Morse, "Theoretical and experimental studies of CO2 laser evaporation of clouds," *Journal of Applied Physics*, vol. 70, no. 8, 1991.

31. J. D. Pendleton, "Water droplets irradiated by a pulsed CO2 laser: comparison of computed temperature contours with explosive vaporization patterns.," *Applied optics*, vol. 24, no. 11, pp. 1631–1637, 1985.

32. A. P. Prishivalko and S. T. Leiko, "Radiative heating and evaporation of droplets," *Journal of Applied Spectroscopy*, vol. 33, pp. 1137–1143, 10 1980.

33. V. P. Skripov, *Metastable liquids.* J. Wiley, 1974.

34. R. Cole, "Boiling Nucleation," *Advances in Heat Transfer*, vol. 10, pp. 85–166, 1974.

35. J. G. Eberhart, "The thermodynamic and the kinetic limits of superheat of a liquid," *Journal of Colloid and Interface Science*, vol. 56, pp. 262–269, 8 1976.

36. B. S. Park, a. Biswas, R. L. Armstrong, and R. G. Pinnick, "Delay of explosive vaporization in pulsed laser-heated droplets.," *Optics letters*, vol. 15, no. 4, pp. 206–208, 1990.

37. A. P. Prishivalko, "Heating and destruction of water drops on exposure to radiation with inhomogeneous internal heat evolution," *Soviet Physics Journal*, vol. 26, pp. 142–148, 1983.

38. P. Sprangle, E. Esarey, and A. Ting, "Nonlinear theory of intense laser-plasma interactions," *Physical Review Letters*, vol. 64, pp. 2011–2014, 4 1990.

39. A. Biswas, H. Latifi, P. Shah, L. J. Radziemski, and R. L. Armstrong, "Time-resolved spectroscopy of plasmas initiated on single, levitated aerosol droplets," *Optics Letters*, vol. 12, no. 5, pp. 313–315, 1987.

40. J. H. Eickmans, W.-F. Hsieh, and R. K. Chang, "Laser-induced explosion of H_2O droplets: spatially resolved spectra," *Optics Letters*, vol. 12, p. 22, 1 1987.

41. M. Z. Martin, M.-D. Cheng, and R. C. Martin, "Aerosol Measurement by Laser-Induced Plasma Technique: A Review," *Aerosol Science & Technology Aerosol Science and Technology*, vol. 316, no. 31, 1999.

42. D. L. Carroll, "Overview of high energy lasers: past, present, and future," in *Proc. of 42nd AIAA Plasmadynamics and Laser Conf*, vol. 3102, 2011.

43. M. D. Perry, D. Pennington, B. C. Stuart, G. Tietbohl, J. A. Britten, C. Brown, S. Herman, B. Golick, M. Kartz, J. Miller, and others, "Petawatt laser pulses," *Optics Letters*, vol. 24, no. 3, pp. 160–162, 1999.

44. Y. Sentoku, T. V. Liseikina, T. Z. Esirkepov, F. Califano, N. M. Naumova, Y. Ueshima, V. A. Vshivkov, Y. Kato, K. Mima, K. Nishihara, and others, "High density collimated beams of relativistic ions produced by petawatt laser pulses in plasmas," *Physical Review E*, vol. 62, no. 5, p. 7271, 2000.

45. "Airborne Laser System (ABL) YAL 1A - Airforce Technology."

46. B. Thompson, S. Davis, W. McDermott, M. Heaven, N. Sabotinov, A. Hill, V. Malkov, A. Boreysho, K. Abramski, and A. Savin, *Gas Lasers*. Optical Science and Engineering, Boca Raton: CRC Press, 2006.

47. R. L. Armstrong, P. J. O'Rourke, and A. Zardecki, "Vaporization of irradiated droplets," *Physics of Fluids*, vol. 29, no. 11, pp. 3573–3580, 1986.

48. R. R. Rogers and M. K. Yau, *A Short Course in Cloud Physics*. Butterworth-Heinemann, 3rd ed., 1996.

49. P. E. Ciddor, "Refractive index of air: new equations for the visible and near infrared," *Appl. Opt.*, vol. 35, pp. 1566–1573, 3 1996.

50. K. Novak, *Numerical Methods for Scientific Computing*. lulu.com, 2017.

REPORT DOCUMENTATION PAGE

Form Approved
OMB No. 0704–0188

1. REPORT DATE *(DD–MM–YYYY)*	2. REPORT TYPE	3. DATES COVERED *(From — To)*
22-03-2018	Master's Thesis	Sept 2016 — Mar 2018

4. TITLE AND SUBTITLE

Simulation and Modeling of
High Energy Laser-Induced
Droplet Shattering in Clouds

5a. CONTRACT NUMBER

5b. GRANT NUMBER

5c. PROGRAM ELEMENT NUMBER

6. AUTHOR(S)

Andrew P. Lawrence

5d. PROJECT NUMBER

5e. TASK NUMBER

5f. WORK UNIT NUMBER

7. PERFORMING ORGANIZATION NAME(S) AND ADDRESS(ES)

Air Force Institute of Technology
Graduate School of Engineering and Management (AFIT/EN)
2950 Hobson Way
WPAFB OH 45433-7765

8. PERFORMING ORGANIZATION REPORT NUMBER

AFIT-ENC-MS-18-M-003

9. SPONSORING / MONITORING AGENCY NAME(S) AND ADDRESS(ES)

10. SPONSOR/MONITOR'S ACRONYM(S)

11. SPONSOR/MONITOR'S REPORT NUMBER(S)

12. DISTRIBUTION / AVAILABILITY STATEMENT

DISTRIBUTION STATEMENT A:
APPROVED FOR PUBLIC RELEASE; DISTRIBUTION UNLIMITED.

13. SUPPLEMENTARY NOTES

14. ABSTRACT

The process of a megawatt laser passing through a cloud is modeled. Specifically, the potential for droplet shattering is explored as a method for clearing a path through a cloud through which a second laser may be sent unobstructed. The paraxial approximation, an approximation to Maxwell's equations, is used to model the beam propagation. The simplified cloud model has assumed a distribution of pure, timescale restricted, droplets evenly distributed with uniform radius and initial temperature. All of the radiative heating is assumed to heat the droplet, neglecting radius change and vaporization based upon characteristic time scales. A 1+1 dimensional model is solved analytically over time and used to verify a numerical model which is then scaled up and applied to the 2+1-dimensional, radially symmetric case. The process is shown to create a cleared channel in a realistic amount of time given the constraining assumptions.

15. SUBJECT TERMS

Laser, HEL, Cloud, Droplet, Shattering

16. SECURITY CLASSIFICATION OF:			17. LIMITATION OF ABSTRACT	18. NUMBER OF PAGES	19a. NAME OF RESPONSIBLE PERSON
a. REPORT	b. ABSTRACT	c. THIS PAGE			Dr. Benjamin Akers, AFIT/ENC
U	U	U	U	45	19b. TELEPHONE NUMBER *(include area code)* (937) 255-3636 x4522;benjamin.akers@afit.edu

Standard Form 298 (Rev. 8–98)
Prescribed by ANSI Std. Z39.18